Control & Manipulation of Electron Beams

Philippe Piot

Department of Physics and Northern Illinois Center for Accelerator & Detector Development, Northern Illinois University, DeKalb,IL 60115 USA
Accelerator Physics Center, Fermi National Accelerator Laboratory, Batavia, IL 60510, USA

Abstract. The concepts of the advanced accelerators and light source rely on the production of bright electron beams. The rms areas of the beam phase space often need to be tailored to the specific applications. Furthermore, a new class of the forefront research calls for detailed specific distribution such as the particle density in the time coordinate. Several groups are tackling these various challenges and in this report we attempt to give a review of the state-of-the-art of the control and manipulation of the electron beams.

Keywords: high brightness electron beams, phase space manipulation,
PACS: 43.35.Ei, 78.60.Mq

INTRODUCTION

Many advanced acceleration and light source concepts rely on the production of bright electron beams. The Generation and transportation of such high brightness electron beams at low energy are challenging due to the nonlinear space charge forces. One recently explored approach targets at generating idealized particle distributions capable of providing linear space charge forces thus preserving beam emittances; however, the technique is not without its limitations. In some other applications, it is advantageous or even necessary to "repartition" the six-dimensional phase space to individually "match" the desired two-dimensional phase spaces. Finally, there are other applications, such as the plasma wakefield accelerator (PWFA), or dielectric wakefield accelerator (DWFA) schemes, whose performances (measured in term of the "transformer ratio") could be considerably enhanced if driven by a linearly ramped bunch or a train of bunches with linearly increasing charge. A micro-bunched electron beam could also has application in the production of superradiant radiation. In this report we review recent developments in the control and manipulation of electron beams. We classify the various manipulation mechanisms in three categories: (1) shaping at-birth, (2) correlation techniques, and (3) exchange between the phase spaces associated to two degrees of freedoms.

SHAPING AT-BIRTH

Some electron emission mechanisms offer, in principle, the possibility to tailor the electron beam during the creation process. In photoemission electron sources, the spatial distribution of the photoemitted electron bunch mirrors the intensity distribution of the photocathode drive laser, provided the time response associated to the photoemission process is much shorter than the laser pulse duration. In an effort to mitigate non linear

space charge forces (which are responsible for emittance dilution), several types of distribution have been considered. An ideal distribution providing linear space charge fields ($E_r \propto r$ and $E_z \propto z$) is the uniformly populated 3D ellipsoid. A method for producing 3D ellipsoid bunch was recently proposed [1] and demonstrated in rf-guns using metallic cathodes [2, 3]. The scheme, initially suggested in Reference [4], relies on the self expansion of a bunch under the influence of its space charge fields. It was shown that an ultrashort laser pulse, with proper transverse distribution, impinging upon a fast-response photocathode could produce a bunch that eventually equilibrates to a 3D ellipsoid provided

$$\frac{eE_0\tau_l}{mc} \ll \frac{\sigma_0}{\varepsilon_0 E_0} \ll 1, \tag{1}$$

where e, m, c and ε_0 are respectively the unit charge, electron rest mass, velocity of light and electric permittivity of vacuum, σ_0 is the surface charge density and E_0 is the peak electric field on the photocathode. In practice, e.g. in a rf gun operating with high ($\sim$nC) bunch charges, there are significant deteriorations of the ellipsoidal character of the distribution due to the cathode image charges. However for most applications the 3D ellipsoid shows significant improvement in beam brightness over other commonly considered distributions, this leads to the adoption of such operation mode by several projects [5]. A disadvantage of this self-generating method to produce a 3D ellipsoid is the lack of control over the bunch duration. To address this limitation the use a 3D-ellipsoid-shaped photocathode-drive laser was proposed [6]. This type of pulse shaping is efficient as long as the time scale of the required distribution is larger than the photoemission response time. Several techniques have been explored to obtain a 3D-ellipsoid laser pulse. Spectral shaping is, in principle, the most straightforward. A temporal pulse stacker that stacks Gaussian pulses with different intensities and transverse sizes is also a potential candidate [6]. The use of silica fiber bundle and deformable mirrors is being investigated as possible shapers [7]. Finally the spatiotemporal coupling of the laser dynamics via chromatic aberration in an optical lens has been shown to be a feasible way to generate 3D ellispoid [8].

The generation of a 3D ellipsoid is generally non-trivial. What has been more popular is the uniformly populated cylinder distribution with small transverse-to-longitudinal aspect ratio in the reference frame $\sigma_\perp/(\gamma\sigma_{||}) \ll 1$ (with γ being the Lorentz factor and $\sigma_{\perp,||}$ the transverse/longitudinal rms sizes in the laboratory frame) has been more popular. The cylinder distribution does in principle support linear space charge fields. In practice however space charge-induced erosion significantly increases the slice emittances associated to the head and tail of the bunch. A comparison of the performances associated to an initial 3D ellispoid and cylinder distribution is shown in Fig. 1.

Cylinder distributions are relatively easy to produce. The pulse stacker technique was initially explored [9], but more promising techniques based on the use of acousto-optic modulator (so-called DAZZLER) have also been investigated [10]. Recently a very simple technique relying on beam shaping based on polarization-dependent group velocity in birefringent crystal was successfully tested for infrared photocathodes drive lasers [11]. The extension of the scheme to uv laser seems straightforward [12].

Besides the production of distributions less prone to phase space dilution due to space charge, shaping at-birth also provides the possibility to tailor distribution along, e.g., the

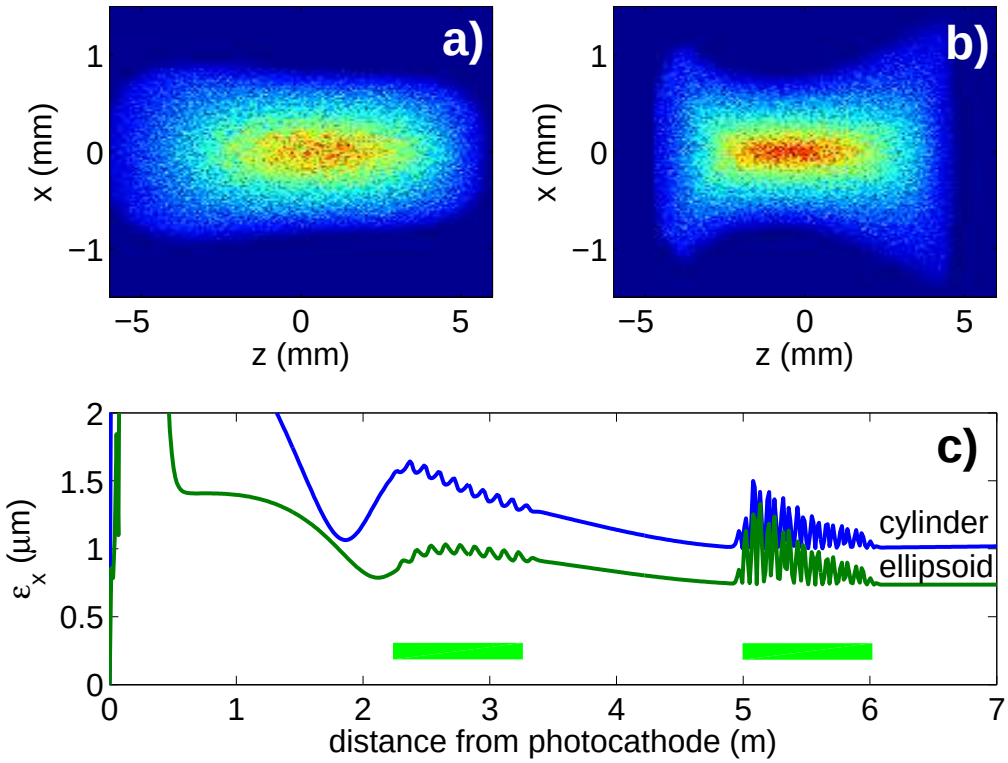

FIGURE 1. Comparison of electron bunch properties generated from an intial 3D ellipsoid and cylinder distributions for the proposed photoinjector for the ILC test accelerator at Fermilab. The images correspond to the transverse density distribution in the (z,x) space for the an initial ellipsoidal (a) and cylinder photocathode laser distribution. The bottom plot show the evolution of the corresponding emittance along the injector beamline. In this particular case, which incorporates the initial thermal emittance for the Cs_2Te cathode, the 3D ellipsoid results in a 30% improvement of emittance compared to the cylinder distribution. The charge is 1 nC and for the two cases presented a genetic optimization algorithm was used to minimize the transverse emittance given the accelerator configuration. The rectangles indicate the locations of the accelerating cavities.

temporal axis. Temporal shaping of the laser distribution has been exploited by several groups to precondition the electron bunch distribution. Reference [13], for instance, discusses the optimum temporal shape of the photocathode drive laser to produce an electron bunch that will eventually acquire, after propagating a multi-GeV linac with all collective effects included, a quasi-constant current distribution as needed for high gain harmonic generation in a seeded FEL. Another application of preconditioned temporal laser shaping is the generation of train microbunch with sub-picosecond spacing. Such trains have applications in the generation of Terahertz coherent radiation [14, 15, 16, 17, 18].

CORRELATION TECHNIQUES

Correlations within one degree of freedom are often used to manipulate a beam (e.g. transverse and longitudinal focusing). Nonlinear correlations within one degree of freedom can be exploited to shape one of the associated projections. An example stems from magnetic bunch compression. We consider the linac located upstream of the magnetic compressor to be composed of accelerating modules of different frequencies f_n with associated accelerating voltages $V_{rf,n}$ and phases φ_n. The final fractional momentum spread of an electron with initial coordinates (z_0, δ_0) in the longitudinal phase is

$$\delta(z) = \frac{E_0}{E_f}\delta_0(z) + \frac{e}{E_f}\sum_{n=1}^{N}\frac{V_{rf,n}}{E_f}[\cos(k_n z + \varphi_n) - \cos(\varphi_n)], \quad (2)$$

where $k_n \equiv 2\pi c f_n$ and $f_n = nf$ (n is an integer and $f \equiv f_1$ is the fundamental frequency). A simple example of usually unwanted effect is the acceleration of a "long" bunch ($\sigma_z \ll 2\pi/\lambda$ violated) in the linac upstream of the bunch compressor. In such case the quadratic distortion ($\delta \propto k_1 z^2$) results in a banana shape bunch current downstream of the compressor. In this particular case the phase space is generally linearized using, e.g., a third harmonic cavity to yield a higher peak current [19].

An example demonstrating the generation of linearly ramped bunch using one harmonic frequency ($n = 3$) is shown in Fig. 2. The current profile distribution can be approximately linearly ramped by the proper choice of the phase and amplitude of the 3rd harmonic with respect to the fundamental accelerating linac. The introduction of a large number of higher harmonic accelerating cavities could provide a way to arbitrarily synthesize any desired shapes for the projection in one degree of freedom.

In practice the introduction of a large number of harmonic is difficult, e.g. due to the need of associated hardware (klystrons etc.. operating at the desired frequencies). An alternative technique is the manipulation of the longitudinal phase space by using coupling it with one of the transverse phase spaces. An illustration of such an implementation is described and demonstrated in Reference [20]. The sextupoles located in a dispersive section of a dogleg beamline were used to introduce a second order path length dependence on fractional energy spread ($z \simeq R_{56}\delta + T_{566}\delta^2$). It was shown that such a simple technique could be used to generate linearly ramped current bunches as needed for enhancing the transformer ratio of a planned PWFA experiment. Although the technique is relatively simple in its implementation, it introduces nonlinear coupling term(s) between the longitudinal and the transverse phase space, which generally result in transverse emittance growth. A similar method to tailor the energy distribution of a high power electron beam in an energy-recovering linac was also described in Reference [21]. Coupling between two degrees of freedom can also be used to temporally shape the beam via interceptive technique. Reference [23] demonstrates how a multi-slit mask located at a high dispersion point of a dispersionless dogleg compressor could generate a train of sub-picosecond electron bunches. Further improvement of the mask could also tailor the overall envelope of the micro-bunch train, e.g. to generate a bunch train with linearly ramped current.

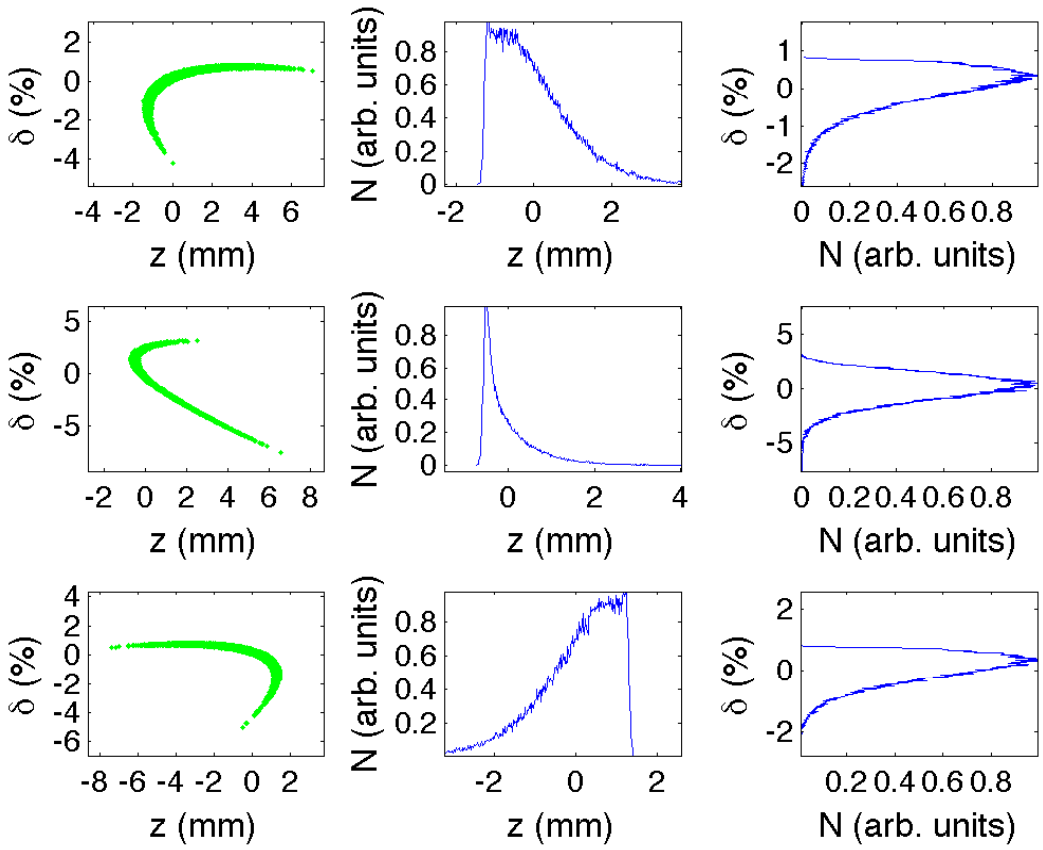

FIGURE 2. Example of nonlinear distortion of the longitudinal phase space and corresponding projections. In this example an electron bunch is accelerated in a linac operating at 1.3 GHz followed by a 3.9 GHz accelerating section and a magnetic chicane. The three rows correspond to three settings of phases, amplitudes and R_{56} for the considered beamline. The three columns respectively show the longitudinal phase space downstream of the beamline, and the corresponding longitudinal and energy projection. The tail of the bunch correspond to $z > 0$ in these plots.

Finally the interaction of an electron beam with an electromagnetic wave (wavelength $\ll$ the bunch length) can naturally produce a train of attosecond bunches as for instance in an inverse free-electron laser (IFEL), either by ballistic bunching or via a miniature magnetic bunch compressor located downstream of the IFEL [22].

PHASE SPACE MANIPULATIONS WITHIN TWO DEGREES OF FREEDOM

A new class of phase space manipulations, capable of repartitioning the phase spaces between two degrees of freedom, have recently emerged. These schemes include the generation of flat beam with certain transverse emittance ratio [24] and the exchange of emittance between one of the transverse and longitudinal phase spaces [33].

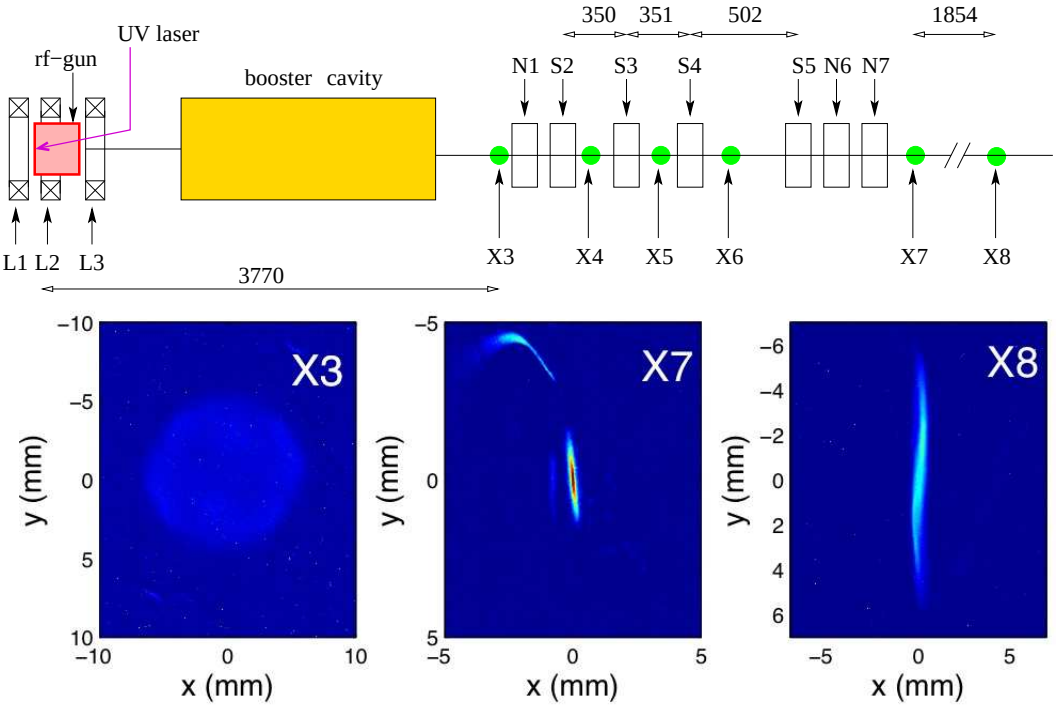

FIGURE 3. Proof-of-principle flat beam experiment at the Fermilab's A0 photoinjector. The top schematic shows the experimental set-up. The skew quadrupole used to generate the flat beam are S1, S2, and S3. The indicated distance are in mm and the X's stand for screens. The bottom pictures show the transverse beam distribution before (on screen X3), just downstream (X7) the round-to-flat beam transformation and after a 2 m drift (X8). The beam transverse distribution remains upright and its aspect ratio does not significantly change between X7 and X8, which indicates of a high transverse emittance asymmetry. The measured emittance ratio was $\varepsilon_x/\varepsilon_y = 100 \pm 20$.

In the flat beam production scheme, the photocathode is immersed in an axial magnetic field. The beam is thereby produced in the presence of a significant longitudinal magnetic field and has an average angular momentum given by $\langle L \rangle = eB_0\sigma_c^2$, where B_0 the magnetic field on the photocathode surface, and σ_c the root-mean-square (rms) transverse size of the drive-laser spot on the photocathode [25]. As the beam exits the solenoidal field, the angular momentum is purely kinetic resulting in a beam coupled in the two transverse planes. Three skew quadrupoles in the beamline can apply a proper total torque needed to cancel the angular momentum [26, 27] as illustrated in Fig. 3. As a result, the beam final transverse emittance are given by

$$\varepsilon_n^{\pm} = \sqrt{(\varepsilon_n^u)^2 + (\beta\gamma\mathscr{L})^2} \pm (\beta\gamma\mathscr{L}) \overset{\beta\gamma\mathscr{L}\gg\varepsilon_n^u}{\longrightarrow} \begin{cases} \varepsilon_n^+ \simeq 2\beta\gamma\mathscr{L} \\ \varepsilon_n^- \simeq \frac{(\varepsilon_n^u)^2}{2\beta\gamma\mathscr{L}} \end{cases}, \tag{3}$$

where $\varepsilon_n^u = \beta\gamma\varepsilon_u$ is the normalized uncorrelated emittance of the magnetized beam prior to the transformer, β andγ the Lorentz factors, $\mathscr{L} \equiv \langle L \rangle / 2p_z$, and p_z is the longitudinal momentum. Note that $\varepsilon_n^+\varepsilon_n^- = (\varepsilon_n^u)^2$. It is worthwhile noting that the amount of emittance exchange can be tuned using the axial magnetic field on the cathode, this

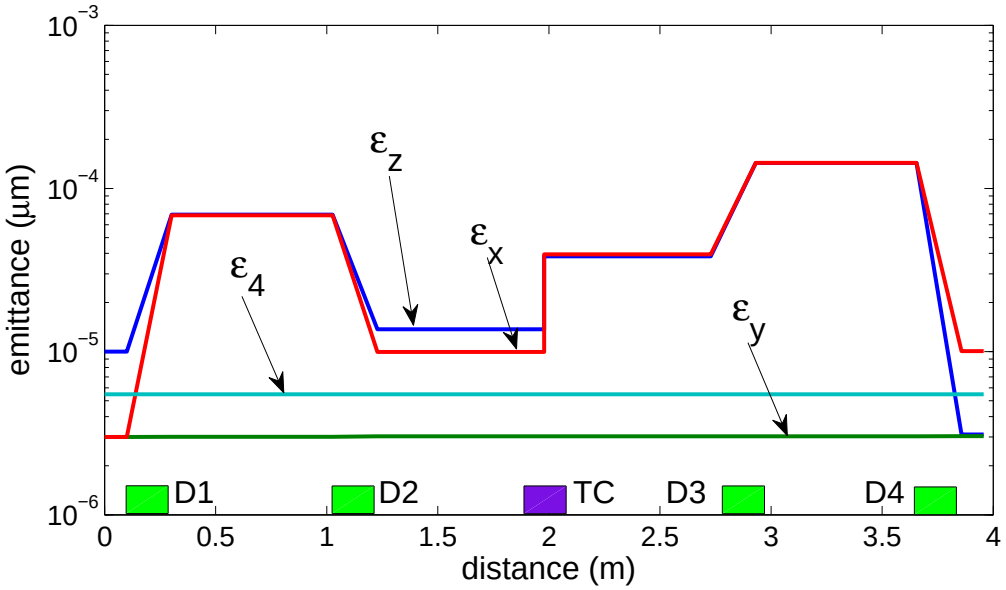

FIGURE 4. Evolution of the two-dimensional emittances in an ideal emittance exchanger. The emittance exchanger swaps the horizontal emittance with the longitudinal emittance. In this example, an incoming beam with emittances $(\varepsilon_{x,0}, \varepsilon_{y,0}, \varepsilon_{z,0}) = (3,3,10)$ μm is converted, downstream of the exchanger, into a beam with emittance $(\varepsilon_x, \varepsilon_y, \varepsilon_z) = (10,3,3)$ μm. . The diagram pictorially represents the emittance exchanger: the green rectangle (D1, D2, D3, and D4) stand for dipoles and the magenta rectangle (TC) for deflecting mode cavity. In this idealized simulation the cavity is assumed to be a thin lens. The four-dimensional emittance is defined as $\varepsilon_4 \equiv \det[\Sigma_4]^{1/4}$ where Σ_4 is the beam matrix in the (x, x', z, δ) sub trace space.

is possible because the beam is born in a magnetic field and therefore sees only one fringe field region of the solenoid: the corresponding "half-matrix" of the solenoid is non-simplectic. To date beams with transverse emittance ratio of ~ 100 have been experimentally demonstrated [28, 29] in a photoinjector; see Fig. 3. Improving the emittance ratio and the associated peak current is one of the goals for the next generation experiments. If successful, the production of high peak current sheet beam could be used in slab dielectric structure [30] and/or novel radiation source such as an image charge undulators [31].

Phase space exchange between the transverse and the longitudinal degrees of freedom is also possible. The technique was first suggested in Reference [32] and latter rediscovered and explored as a possible way to suppress the microbunching instability in the Linac Coherent Light Source (LCLS) [33]. As discussed in References [34, 35] a deflecting mode resonant cavity flanked by two dogleg can act as an emittance exchanger between the longitudinal and the bending-plane transverse degree-of-freedom. Given the dispersion value generated by one dogleg, η, and the deflecting cavity strength κ, the

total transverse matrix of the exchanger is

$$M = M_{DL} M_{CAV} M_{DL} = \begin{bmatrix} A & B \\ C & D \end{bmatrix}. \tag{4}$$

Under the thin lens approximation, $A = B = 0$. When the condition $\kappa = -1/\eta$ is satisfied, a perfect emittance exchange is achieved [34]; see Fig. 4. For the general non-thin lens case, the final emittances are approximately [33, 36]

$$\begin{bmatrix} \varepsilon_x^2 \\ \varepsilon_z^2 \end{bmatrix} = \begin{bmatrix} |A|^2 & |B^2| \\ |C^2| & |D^2| \end{bmatrix} \begin{bmatrix} \varepsilon_{x,0}^2 \\ \varepsilon_{z,0}^2 \end{bmatrix} + \lambda^2 \varepsilon_{x,0} \varepsilon_{z,0} I, \tag{5}$$

where I is the 2×2 identity matrix and $\lambda^2 > 0$ is a function of η, R_{56} (the longitudinal dispersion of the dogleg), and the incoming Courant-Snyder parameters. It can generally be minimized, e.g. by choosing the proper initial time-energy chirp, making in practice the emittance exchange possible [36, 37]. Two independent proof-of-principle experiments to demonstrate such an exchange are being pursued at Fermilab and Argonne [37, 38]. An application of this phase space exchange to produce a train of microbunches is discussed in Reference [39].

ACKNOWLEDGMENTS

I am indebt to the AAC08 organizing committee for the invitation to present this paper. I would like to acknowledge fruitful discussions with numerous colleagues in particular with K.-J. Kim, Y. Li, R. Legg, J. G. Power, and Y.-E Sun. This work was supported by the US Department of Energy under Contract No. DE-AC02-76CH00300 with Northern Illinois University and under contract No. DE-AC02-07CH11359 with the Fermi Research Alliance, LLC.

REFERENCES

1. O. J. Luiten, *et al.*, *Phys. Rev. Lett.* **93**, 094802 (2004).
2. P. Musumeci, *et al.*, *Phys. Rev. Lett.* **101**, 244801 (2008).
3. W. Op't Root, *et al.*, Proc. 13th Advanced Accelerator Concepts Workshop, Santa Cruz, CA (2008).
4. L. Serafini, AIP Conf. Proc. **413**, 321 (1997).
5. R. Legg, W. Graves, T. Grimm, and P. Piot, Proc. of EPAC 2008, Genova (Italy), 469 (2008).
6. C. Limborg-Deprey, and P. Bolton, *Nucl. Instr. Meth.* **A 557**, 106 (2006).
7. H. Tomizawa, *et al.*, *Nucl. Instr. Meth.* **A 557**, 117 (2006).
8. Y. Li, and J. W. Lewellen, *Phys. Rev. Lett.* **100**, 074801 (2008).
9. J. Li, R. Tikhoplav, A. C. Melissinos, *Nucl. Instr. Meth.* **A 564**, p. 57 (2006).
10. C. Vicario, *et al.* Proc. of EPAC 2004, Lucerne (Switzerland), 1301 (2004).
11. I Bazarov, *et al.*, *Phys. Rev. ST Accel. Beams* **11**, 040702 (2008).
12. J. G. Power *et al.* , Proc. 13th Advanced Accelerator Concepts Workshop, Santa Cruz, CA (2008).
13. M. Cornacchia, S. Di Mitri, G. Penco, and A. Zholents, *Phys. Rev. ST Accel. Beams* **9**, 120701 (2006).
14. J. G. Neumann, *et al.*, *Nucl. Instr. Meth.* **A 507**, 498 (2003).
15. M. Bolosco, *et al.*, *Nucl. Instr. Meth.* **A 577**, 409 (2007).
16. Y. Li, and K.-J. Kim, *Appl. Phys. Lett* **92**, 014101 (2008).
17. Y. C. Huang, *et al.*, *International Journal of Modern Physics B*, **21** (3/4), 287 (2007).

18. Y. Li, Y.-E Sun and K.-J. Kim, *Phys. Rev. ST Accel. Beams* **11**, 080701 (2008).
19. T. I. Smith, Proc. of LINAC 1984 (SLAC report num. 303), Stanford, 421 (1984).
20. R. J. England, J. B. Rosenzweig, and G. Travish, *Phys. Rev. Lett.* **100**, 214802 (2008).
21. P. Piot, D. R. Douglas and G. A. Krafft, *Phys. Rev. ST Accel. Beams* **6**, 030702 (2003).
22. C. Sears, *et al.*, *Phys. Rev. ST Accel. Beams* **11**, 061301 (2008).
23. P. Muggli, *et al.*, *Phys. Rev. Lett.* **101**, 054801 (2008).
24. R. Brinkmann, Ya. Derbenev and K. Flöttmann, *Phys. Rev. ST Accel. Beams* **4**, 053501 (2001).
25. Y.-E Sun, *et al.*, *Phys. Rev. ST Accel. Beams* **7**, 123501 (2004).
26. A. Burov, Ya. Derbenev, S. Nagaitsev, *Phys. Rev.* **E 66**, 016503 (2002).
27. K.-J. Kim, *Phys. Rev. ST Accel. Beams* **6**, 104002 (2003).
28. Y.-E Sun, PhD dissertation, University of Chicago (2005).
29. P. Piot, Y.-E Sun, and K.-J. Kim, *Phys. Rev. ST Accel. Beams* **9**, 031001 (2006).
30. A. Tremaine, J. Rosenzweig, and P. Schoessow, *Phys. Rev.* **E 56**, 7204 (1997).
31. Y. Zhang, Ya Derbenev, and R. Li., *Nucl. Instr. Meth.* **A 507**, 459-463 (2003).
32. Y. Orlov et al., Proc. of PAC91, San Francisco, 2838 (1991).
33. M. Cornacchia and P. Emma, *Phys. Rev. ST Accel. Beams* **5**, , 084001 (2002).
34. K.-J. Kim and A. Sessler, AIP Conf. Proc. **821**, p. 115 (2006).
35. P. Emma, Z. Huang, K.-J. Kim, and P. Piot, *Phys. Rev. ST Accel. Beams* **9**, 100702 (2006).
36. Y.-E Sun, *et al*, Proc. of the PAC07, 3441 (2007).
37. M. Rihaoui, *et al.*, Proc. 13th Advanced Accelerator Concepts Workshop, Santa Cruz, CA (2008).
38. R. Fliller, *et al.* , Proc. 13th Advanced Accelerator Concepts Workshop, Santa Cruz, CA (2008).
39. P. Piot, *et al.*, Proc. 13th Advanced Accelerator Concepts Workshop, Santa Cruz, CA (2008).